Sensors and Materials, Vol. 37, No. 7 (2025) 3135–3150
MYU Tokyo

S & M 4108

Optimal Control of Computer Numerical Control Machining Tool Motion in Green Converter Station Based on Multisensor Fusion Data

Yang Li,[1] Guoen Zhou,[1] Jiaqi Xue,[1] Junwei Yang,[2] Wenting Wang,[2,3] and Tianyu Nie[2,4*]

[1]Ultra High Voltage Transmission Company Dali Bureau, China Southern Power Grid Co., Ltd., 671000, China
[2]Longshine Technology Group Co., Ltd., Wuxi 214000, China
[3]Faculty of Civil Aviation and Aeronautics, Kunming University of Science and Technology, Kunming 650500, China
[4]Faculty of Information Engineering and Automation, Kunming University of Science and Technology, Kunming 650500, China

(Received October 25, 2024; accepted July 22, 2025)

Keywords: green converter station, smooth transition, circular interpolation, optimal control

Striving to enhance the efficiency of computer numerical control (CNC) machining tools used in green converter stations, in this paper, we introduce an innovative approach leveraging multisensor fusion data for the optimal control of a machine's motion along each coordinate axis. The proposed method focuses on the optimal control of the machine's motion along each coordinate axis, while considering constraints of precision, speed, and acceleration. A trajectory planning method synthesizing linear interpolation, circular interpolation, and a novel circular arc transfer algorithm is employed. Unlike traditional techniques, our S-curve acceleration and deceleration control model for path segments does not mandate identical start and end speeds for a single path. The model's efficacy was validated through simulation experiments on a rounded rectangular cutting path, with sensor data simulating real-time machining conditions. The results demonstrated that accounting for instantaneous machining speed and acceleration aids in achieving maximum machining speed more rapidly. Our sensor-informed optimal control algorithm ensured a seamless kinematic transition at the path's intersection, minimizing abrupt speed changes, which elevated the efficiency of the CNC tool's motion, markedly reducing the process time. This contribution serves as a major advancement in optimizing CNC machining, promising considerable time efficiency in production.

1. Introduction

Machine tools play a key role in the equipment manufacturing of green converter stations, which are facilities designed for high-efficiency energy conversion in power transmission systems, often integrating environmentally friendly technologies. For example, high-precision machine tools are essential for processing components such as the iron core and winding of a converter transformer. They can accurately cut silicon steel sheets for the iron core with

*Corresponding author: e-mail: 909778395@qq.com
https://doi.org/10.18494/SAM5630

ISSN 0914-4935

thickness tolerance within ±0.03 mm and perform high-precision wire drawing processing for copper conductors in winding to meet the high-efficiency requirements of converter transformers. Computer numerical control (CNC) machining technology is evolving towards high speed, efficiency, and precision, driven by the integration of sensor networks that monitor real-time tool motion and machining states. High-speed machining requires rapid operation and precise, swift stops of machine tool axes.

There are three main research directions. (1) The first improves interpolation methods such as point-by-point comparison and time division,[1,2] which can be enhanced by sensor-based position feedback to reduce interpolation errors. For example, Shu *et al.*[3] proposed an optimization technique for linear interpolation, improving the processing efficiency of a product. (2) The second is using the new S-curve acceleration and deceleration control model to achieve feed speed with the change in the curvature radius region and an adaptive change.[4,5] Researchers such as Xiao *et al.*[6] proposed improved algorithms based on the algorithm of inserting a circular arc path between adjacent linear segments of the machining trajectory. Lu and Chen [7] proposed a genetic-algorithm-based S-curve acc/dec scheme. (3) The third is inserting transition curves to improve speed and smoothness. Wang *et al.*[8] and others proposed pick-and-place path [9,10] trajectory planning to improve operational efficiency.[11] Analytical transformation algorithms are proposed to smooth corners to generate curvilinear continuous toolpaths in real time.[12–14]

In this paper, by inserting the arc transfer model and combining it with the new S-curve acceleration and deceleration control model, we integrate multisensor fusion data (e.g., position, velocity, acceleration sensors) to perform path forward-looking planning under CNC machine tool limitations. This sensor-driven approach enables the optimal control of machining tools by adapting to real-time operational constraints and ensuring precision throughout the machining process.

2. Optimal Control Model of Linear Machining Segment

2.1 Optimization model of straight line machining segment based on point-by-point comparison method

The machining tool path is a series of straight line segments. Length is a multiple of resolution, affecting a tool's velocity and acceleration. For plane-type machining surfaces, the tool path is typically composed of polyline segments, which requires the precise coordination of multi-axis motion.

Considering the problem of the polyline segment formed by the connection of two straight lines, the end point of the point-by-point comparison interpolation method is defined as the point closest to the intersection of the polyline. This end point is then used as the starting point. From this starting point, interpolation calculation is performed on another straight line. This process allows for obtaining an interpolation calculation method for two adjacent polyline segments. Figure 1 shows the interpolation feed chart for linear segments, illustrating the feed process of the point-by-point comparison method. Figure 2 presents the linear interpolation of the point-by-point comparison method, detailing coordinate changes during machining.

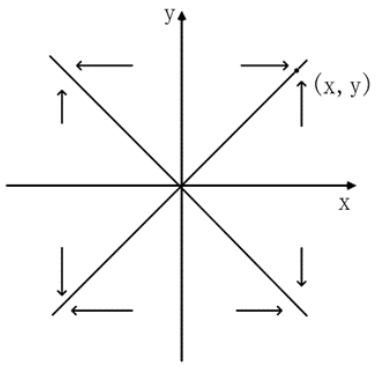

Fig. 1. Interpolation feed chart for linear segments.

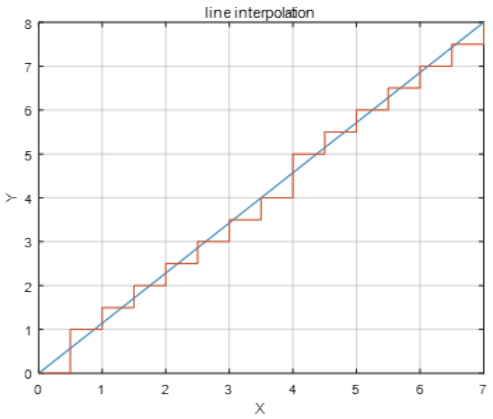

Fig. 2. (Color online) Point-by-point comparison method.

2.2 Control model of tool moving in a straight line

A new type of S-type acceleration and deceleration control method can be adopted for the straight section of the processing profile. S is set to the given displacement of the line segment, and $S = S_{up} + S_w + S_{down}$ (where S_{up} is the displacement during acceleration, S_w is the displacement during the uniform speed process, and S_{down} is the displacement during deceleration), V is the velocity, a is the acceleration, J is the jerk, V_s is the initial velocity, and V_e is the final velocity. The acceleration and deceleration times are the same as T_1 and T_2, and the constant speed time is T_3.

The formula for calculating displacement is

$$S(t)=\begin{cases} V_s t+\dfrac{1}{6}Jt^3,\ t\in(0,T_1] \\ \left(V_s+JT_1^2\right)t-\dfrac{1}{6}J(t-2T_1)^3-JT_1^3,\ t\in(T_1,2T_1] \\ \left(V_s+JT_1^2\right)t-JT_1^3,\ t\in(2T_1,2T_1+T_3] \\ \left(V_s+JT_1^2\right)t-\dfrac{1}{6}J(t-2T_1-T_3)^3-JT_1^3,\ t\in(2T_1+T_3,2T_1+T_3+T_2] \\ \left(V_s+J\left(T_1^2-T_2^2\right)\right)t+\dfrac{1}{6}J(t-2T_1-T_3-T_2)^3+JT_2^2\left(2T_1+T_3+T_2\right), \\ -JT_1^3,\ t\in(2T_1+T_3+T_2,2T_1+T_3+2T_2]. \end{cases} \tag{1}$$

When $t = 2T_1 + T_3 + 2T_2$, we obtain $V_e = V_s + J\left(T_1^2 - T_2^2\right)$, i.e., by finding the value of either one, we can find the value of the other. We solve for T_1, T_2 in two cases below.

1. If $S_w \geq 0$, we can obtain

$$V_{max} = V_s + JT_1^2 \cdot \tag{2}$$

Then, $T_1 = \sqrt{(V_{max} - V_s)/J}$, where $V_{max} = V_e + JT_2^2$, and $T_2 = \sqrt{(V_{max} - V_e)/J}$. However,

$$\begin{cases} S_{up} = 2V_s T_1 + JT_1^3, \\ S_w = \left(V_s + JT_1^2\right) T_3, \\ S_{down} = 2V_e T_2 + JT_2^3. \end{cases} \tag{3}$$

2. If $S_w < 0$, we can consider that there is no uniform speed zone, so T_3 is 0 and the maximum speed V_{max} cannot be reached and $t = 2T_1 + T_3 + 2T_2$.

$$S(t) = 2V_e T_2 + JT_2^3 + \left(V_e + V_s + JT_2^2\right)\sqrt{(V_e - V_s)/J + T_2^2} \tag{4}$$

If T_2 is regarded as a variable in the above equation, then $S(t)$ can be taken as a function about T_2, denoted as $S(T_2)$, which is monotonically increasing with respect to the interval $T_2 \in [0, \infty)$. The upper limit of T_2 values obtained from the above equation is $\sqrt{(V_{max} - V_e)/J}$.

When $V_e \geq V_s$, the minimum T_2 value is 0, and its possible value interval is $[0, \sqrt{(V_{max} - V_e)/J}]$. Therefore, if there is a positive solution for the given displacement $S > (V_e + V_s)\sqrt{(V_e - V_s)/J}$, let $S(T_2) = S$ adopt the bisection method to solve T_2; otherwise, reselect the initial velocity V_s and final velocity V_e.

When $V_e < V_s$, the T_2 minimum value $\sqrt{(V_s - V_e)/J}$ obtained is $(V_e - V_s)/J + T_2^2 \geq 0$. Then, the interval of values is $\left[\sqrt{(V_s - V_e)/J}, \sqrt{(V_{max} - V_e)/J}\right]$. Therefore, if the displacement is given as $S > (V_e + V_s)\sqrt{(V_s - V_e)/J}$, T_2, there is a positive solution. Let $S(T_2) = S$, and we use the bisection method to solve T_2; otherwise, reselect the initial velocity V_S and final velocity V_e.

Substituting the obtained T_2, we obtain T_1, and the sum of S_{up}, S_w, S_{down} and T_3 can be obtained. When T_1, T_2, and T_3 are obtained, the speeds of each region can also be determined.

3. Continuous Curve Optimization Model Composed of Straight Line and Circular Arc Segments

3.1 Optimization model of linear machining section

We use the point-by-point comparison method to interpolate the straight line and the new S-type acceleration and deceleration control method to calculate the change in the moving speed of the tool on the linear motion path.

3.2 Optimization model of arc machining segment based on time division method

The working principle of time division interpolation equipment control is to calculate the contour step length according to the feed rate, use it as the chord length for circular interpolation, and calculate coordinate axis feeds. Figure 3 shows the circular interpolation with time division method.

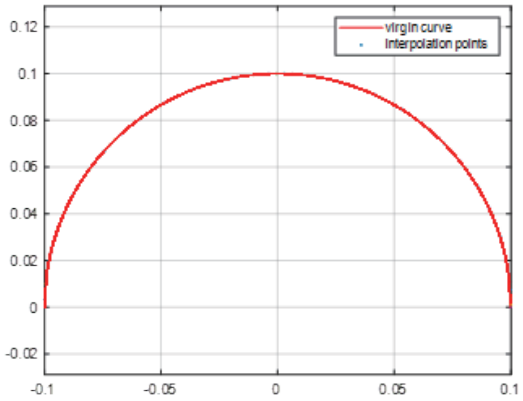

Fig. 3. (Color online) Circular interpolation with time division method.

4. Arc Transfer Optimization Algorithm

4.1 Arc insertion method

In circular interpolation, the inserted transition arc is approximated by discrete linear segments to satisfy machining error constraints, where E_R represents the allowable error of the radius of the inserted arc and E_{rr} indicates the total allowable error at the transition of the trajectory segment as shown in Fig. 4 .

By setting $|AB| = |AC| = d$, $\angle BAO = \theta$, $|AF| = E_{rr}$, and $|EF| = E_R$ from the geometric relationship in the figure, we can obtain

$$\left(\frac{d}{\cos\theta} - d\tan\theta\right) + E_R \geq E_{rr}, \tag{5}$$

$$d \leq \frac{E_{rr} - E_R}{\frac{1}{\cos\theta} - \tan\theta}. \tag{6}$$

We insert arc radius $R = d\tan\theta$. The coordinates of points B, C, and O can be determined according to the coordinates of d, R, E_R, E_{rr} point A.

4.2 Determination of transfer speed

(1) Transfer conditions

To ensure that the change in velocity vector at the transition of the trajectory segment is dispersed into multiple interpolation periods, with T indicating the interpolation period, there should be $v_1 T \leq 2R\cos\theta$, that is,

$$v_1 \leq \frac{2R\cos\theta}{T}. \tag{7}$$

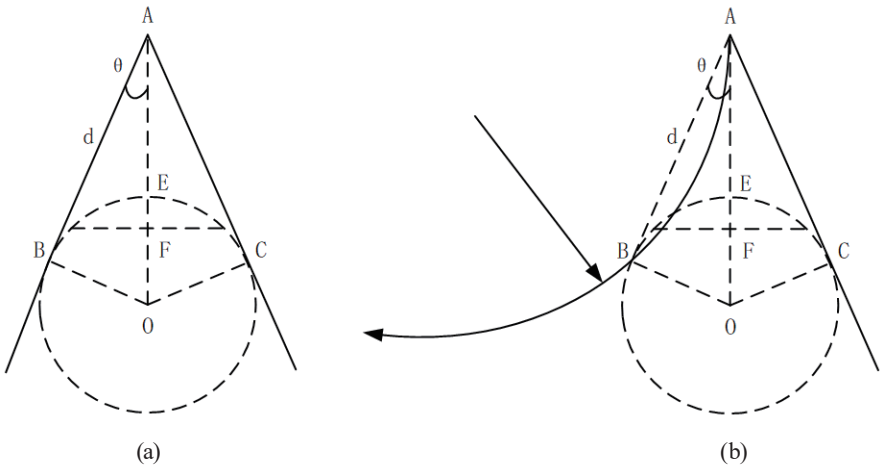

Fig. 4. Schematic diagram of arc insertion: (a) original trajectory and (b) trajectory after arc insertion.

(2) Arc radius error limit

The radius of the arc allows the transfer speed formula determined by the machining error constraints to be used as

$$v_1 \le \frac{2R}{T}\sqrt{1-\left(1-\frac{E_R}{R}\right)^2}\,. \tag{8}$$

When the radius of the inserted arc is large, after simplification, the quadratic term is discarded and expressed as

$$v_2 \le \frac{\sqrt{8RE_R}}{T}\,. \tag{9}$$

(3) Acceleration limit

When the radius of the interpolation arc is large, because the interpolation step is much smaller than the radius of the arc, the corners of two adjacent interpolation steps can be ignored, and the acceleration limitation does not need to be considered. However, in the "arc transfer method," the radius of the inserted arc is small, and it is necessary to consider the acceleration limit. The maximum allowable feed normal acceleration of the machine tool is limited. The relationship between the feed normal acceleration and the feed rate and the radius of the inserted arc is

$$a_n = \frac{V^2}{R}\,. \tag{10}$$

Then, the maximum allowable speed is

$$V_{max} = \sqrt{a_N \times R}\,. \tag{11}$$

Using Eqs. (15) and (16), we can obtain

$$v_3 \in (V, V_{max}) . \tag{12}$$

The transfer speed between tracks using the arc transfer method is determined as

$$v = \min\{v_1, v_2, v_3\} . \tag{13}$$

Let E_{rr} = 2 μm, E_R = 0.9 μm, a = 600 mm/s^2, and T = 1 ms; when the angle shown in Fig. 5 $\theta \in (0^\circ, 90^\circ)$ is the angle between two adjacent track segments $2\theta \in (0^\circ, 180^\circ)$, the transfer speed is calculated according to the above formula, and the v curve is shown in Fig. 5.

5. Experiment

5.1 Data preparation

Figure 6 shows a schematic diagram of a cutting path in the shape of a rounded rectangle. The four corners of the path each consist of 1/4 arcs from a complete circle with a radius of 0.5. The dimensions of the rectangle are 41 × 41 (cm^2). Figure 7 shows the processing speed profile of the rounded rectangular cutting path, showing speed changes at each node.

During real-world machining operations, the tool initiates from the position of node 1 with coordinates (−20.500, −0.000, 0.000) and an instantaneous speed of 0.13 m/min at this point. The tool needs to increase to a maximum speed of 0.19 m/min to move from node 1 to node 2 (−20.500, −17.708, 0.000). Starting from node 2 (−20.500, −17.708, 0.000), the tool moves in a clockwise direction and returns to this point (referenced as node 11), requiring a maximum speed of 1.26, and finally slows down to a termination speed of 0.13 at node 11. Table 1 outlines

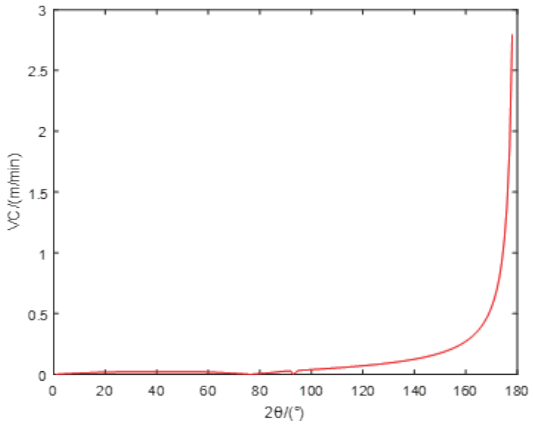

Fig. 5. (Color online) $v - 2\theta$ curve.

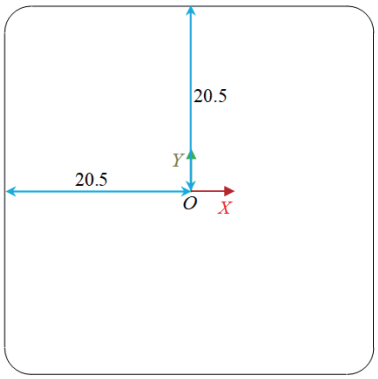

Fig. 6. (Color online) Rounded rectangle cutting path.

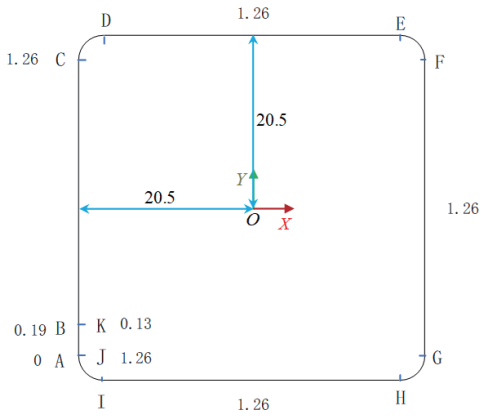

Fig. 7. (Color online) Schematic diagram of the processing speed of the rounded rectangular cutting path.

the required maximum speeds throughout the operation. In the table, the maximum frequency refers to the maximum frequency of the control pulse, which can be overlooked. The corresponding speed denotes the movement speed of the tool, and it is measured in m/min.

During the movement, the limitation conditions of the machine tool for speed, acceleration, jerk, and so forth are as follows.

1. Feed speed V range [V_{min}, V_{max}]: [0.13,6] unit m/min
2. Acceleration range [A_{min}, A_{max}]: [0.02,0.6] unit m/s^2 a
3. Jerk: 300 units mm/s^3 J_{const}
4. Instant start speed V_0: V_0 = 0.13 unit m/min
5. Instant start acceleration a_0: a_0 = 0.02 unit m/s^2
6. Error: ε = 1 μm
7. Resolution: 1/1280 mm

5.2 Optimization model checking

5.2.1 Processing speed of rounded rectangle cutting path

Table 1 outlines the processing speeds for each segment of the rounded rectangular cutting path. For the straight line segment AB, the speed at point A is 0.13 m/min (with the instantaneous start acceleration and start speed considered), the maximum speed of the AB segment is 0.19 m/min, and the speed at point B is 0.19 m/min. From point C to point J, the processing speed is maintained at 1.26 m/min. For the segment from point J to point K, the speed at point J is 1.26 m/min, and the terminal speed at point K is 0.13 m/min. Table 2 shows the analysis of different paths.

5.2.2 Control calculation of rounded rectangle cutting path

For better verification, the following data are provided: J = 300 mm/s^3 = 0.3 m/s^3, AB: V_A = 0, V_B = 0.19 m/min, and V_{max} = 0.19 m/min.

Table 1
Speed requirements for rounded rectangular cutting path processing.

Path node	Node coordinates (*X*, *Y*, *Z*)	Corresponding speed (m/min)
1	(−20.500, −20.000, 0.000)	0.13
2	(−20.500, −17.708, 0.000)	0.19
3	(−20.500, 20.000, 0.000)	1.26
4	(−20.000, 20.500, 0.000)	1.26
5	(20.000, 20.500, 0.000)	1.26
6	(20.500, 20.000, 0.000)	1.26
7	(20.500, −20.000, 0.000)	1.26
8	(20.000, −20.500, 0.000)	1.26
9	(−20.000, −20.500, 0.000)	1.26
10	(−20.500, −20.000, 0.000)	1.26
11	(−20.500, −17.708, 0.000)	0.13

Table 2
Path analysis chart.

Path	Initial speed (m/min)	Final velocity (m/min)	Acceleration time (s)	Deceleration time (s)
Section AB	0	0.19	0.1	0
Section BC	0.19	1.26	0.24	
CJ segment		Uniform motion time is 77.4 s		
JK segment	1.26	0.13		0.25

According to the new S-curve acceleration and deceleration algorithm of the straight line segment, it is assumed that the AB segment has a uniform-speed stage, that is, there is $S_w \geq 0$. It can be obtained as $V_{max} = V_A + JT_1^2$.

Then, $T_1 = \sqrt{(V_{max} - V_A)/J} = \sqrt{0.19/(60 \times 0.3)} = 0.10\,\text{s}$, where $V_{max} = V_e + JT_2^2$, and $T_2 = \sqrt{(V_{max} - V_e)/J} = 0\,\text{s}$. The maximum acceleration, calculated as JT_1 = 0.03 m/s^2, falls within the allowable range of maximum acceleration; the accelerated displacement is $S_{up} = 2V_A T_1 + JT_1^3 = 0.03\,\text{cm}$; the uniform displacement is S_w = 20 − 17.708 − 0.03 = 2.262 cm; the BC segment has an initial speed V_B = 0.19 m/min, V_{max} = 1.26 m/min; and the acceleration time is $T_3 = \sqrt{(V_{max} - V_B)/J} = \sqrt{(1.26 - 0.19)/(60 \times 0.3)} = 0.24\,\text{s}$ and the uniform time is $T_4 = (162.54/100)/1.26/60 = 77.4\,\text{s}$.

5.2.3 Analysis of simulation results

With the proposed algorithm to simulate the rounded rectangular cutting path on MATLAB, the simulation results of the machining speed and machining acceleration of the entire machining process are as shown in Fig. 8. Figure 9 details the machining speed and acceleration changes in the AC segment, where (a) shows the relationship between machining speed and time, and (b) shows the correlation between machining acceleration and time, further verifying the effectiveness of the S-curve acceleration and deceleration control in this segment. Figure 10 presents the machining speed and acceleration curves of the JK segment, with (a) showing the variation in machining speed with time and (b) displaying the change in machining acceleration

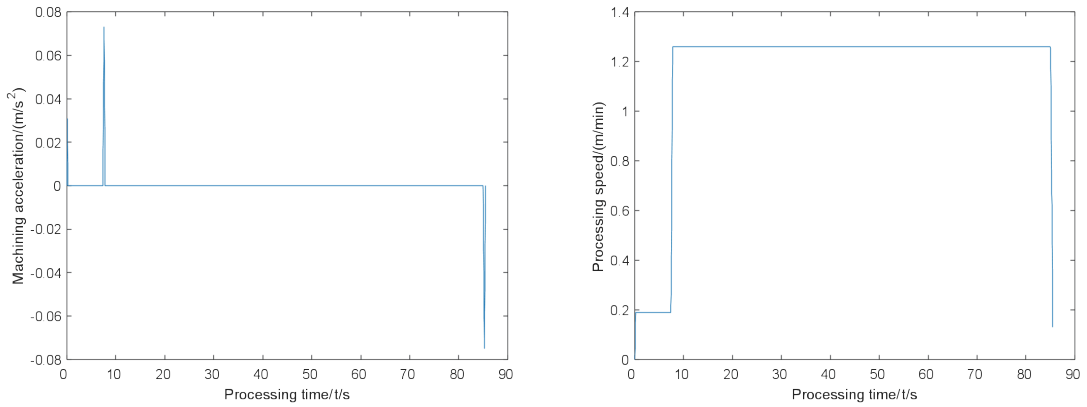

(a) (b)

Fig. 8. (Color online) Processing speed and acceleration curves: (a) total curve of machining speed versus machining time and (b) total curve of machining acceleration versus machining time.

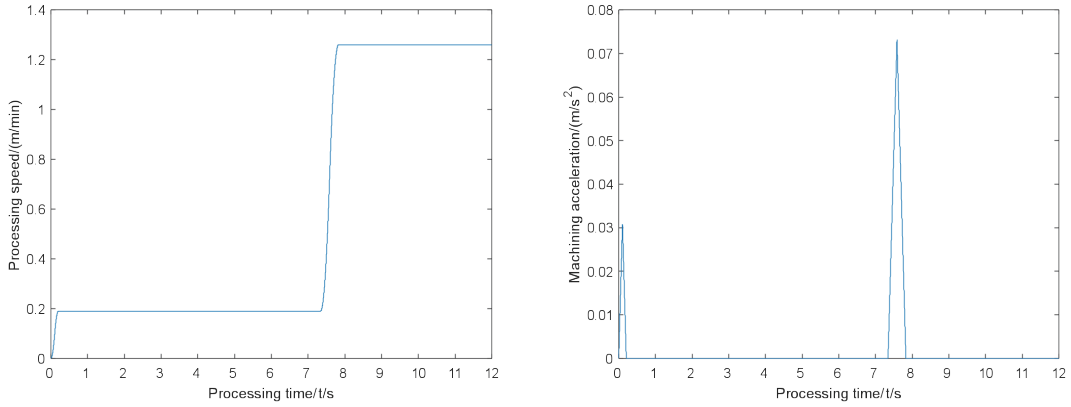

(a) (b)

Fig. 9. (Color online) AC segment machining speed and acceleration curves: (a) curve of machining speed versus machining time in AC section and (b) curve of machining acceleration versus machining time in AC section.

over time, which clearly reflects the deceleration process from 1.26 to 0.13 m/min using the new S-curve acceleration and deceleration method.

5.3 Optimal model checking considering instantaneous startup acceleration and instantaneous startup speed

5.3.1 Optimization model establishment

Consider the instantaneous starting acceleration and the instantaneous starting velocity, that is, the initial acceleration and initial velocity are no longer zero. Let the given initial acceleration

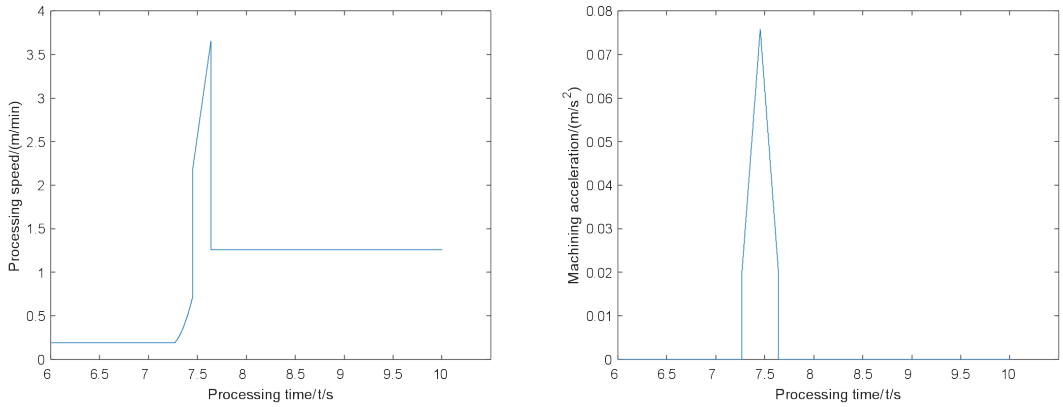

(a) (b)

Fig. 10. (Color online) Processing speed and acceleration curves of JK segment: (a) curve of machining speed versus machining time in JK section and (b) curve of machining acceleration versus machining time in JK section.

be a_0, the initial speed be V_0, and the calculation formulas of its speed and acceleration be as follows.

$$t \in (0, T_1]$$

$$\begin{cases} a_1(t) = Jt \\ V_1(t) = V_0 + a_0 t + \frac{1}{2} J t^2 \\ S_1(t) = V_0 + a_0 t + \frac{1}{2} J t^2 + \frac{1}{6} J t^3 \end{cases} \tag{14}$$

$$t \in (T_1, 2T_1]$$

$$\begin{cases} a_2(t) = a_0 - J(t - T_1) + JT_1 \\ V_2(t) = V_0 + a_0 t + \frac{1}{2} J t^2 + a_0 (t - T_1) \\ S_2(t) = V_0 t + \frac{1}{2} a_0 t^2 + \frac{1}{6} J t^3 + \int_{T_1}^{t} V_2(t)\, dt \end{cases} \tag{15}$$

$$t \in (2T_1, 2T_1 + T_3]$$

$$\begin{cases} a_3 = 0 \\ V_3 = V_2 \end{cases} \tag{16}$$

$$t \in (2T_1 + T_3, 2T_1 + T_3 + T_2]$$

$$\begin{cases} a_4(t) = -a_0 - J\left[t - (2T_1 + T_3)\right] \\ V_4(t) = V_3 + \int_{2T_1+T_3}^{t} a_4 dt \end{cases} \tag{17}$$

$$t \in (2T_1 + T_3 + T_2, 2T_1 + T_3 + 2T_2]$$
$$\begin{cases} a_5(t) = -a_1 - JT_2 + J\left[t - (2T_1 + T_3 + T_2)\right] \\ V_5(t) = V_4 + \int_{2T_1+T_3+T_2}^{t} a_5 dt \end{cases} \tag{18}$$

$$\begin{cases} a_{\max} = a_0 + Jt \\ V_1 = V_0 + a_0 T_1 + \frac{1}{2} J T_1^2 \end{cases} \tag{19}$$

$$T_1 = \frac{-2a_0 + \sqrt{4{a_0}^2 + 4J(V_{\max} - V_0)}}{2J} \tag{20}$$

Using the above formula, according to the arc machining segment method, we can obtain T_1, T_2, and T_3. Once S_{up}, S_w, and S_{down} are obtained, the velocity of each region can also be determined.

5.3.2 Analysis of simulation results

Most of the processes are carried out at the required maximum processing speed, and the total processing time is 85.38 s. Because the initial instantaneous velocity and initial acceleration are considered in this question, the acceleration range is [0.02, 0.6]. Figure 11 shows the overall machining speed and acceleration curves when the initial instantaneous velocity and acceleration are considered: (a) shows the total curve of machining speed versus machining time and (b) shows the total curve of machining acceleration versus machining time, clearly reflecting the dynamic changes throughout the entire process. Figure 12 shows the local machining speed and acceleration curves of the AB segment: (a) depicts the curve of machining speed versus machining time in the AB section and (b) shows the curve of machining acceleration versus machining time in this segment, detailing the start-up phase. Figure 13 shows the local machining speed and acceleration curves of the BC segment: (a) is the curve of machining speed versus machining time in the BC section and (b) is the curve of machining acceleration versus machining time here, demonstrating the acceleration process to the maximum speed. Figure 14 shows the processing speed and acceleration curves of the JK segment: (a) is the curve of machining speed versus machining time in the JK section and (b) is the curve of machining acceleration versus machining time in this segment, reflecting the deceleration process to the terminal speed.

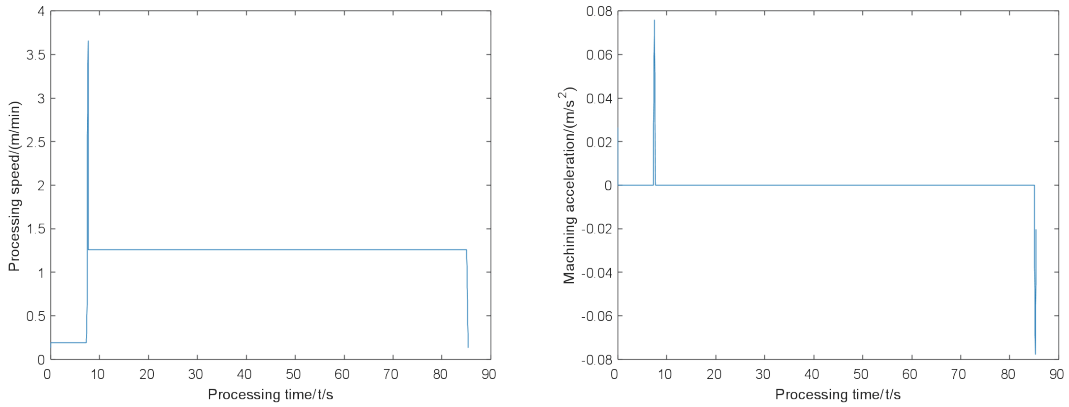

(a) (b)

Fig. 11. (Color online) Processing speed and acceleration curves: (a) total curve of machining speed versus machining time and (b) total curve of machining acceleration versus machining time.

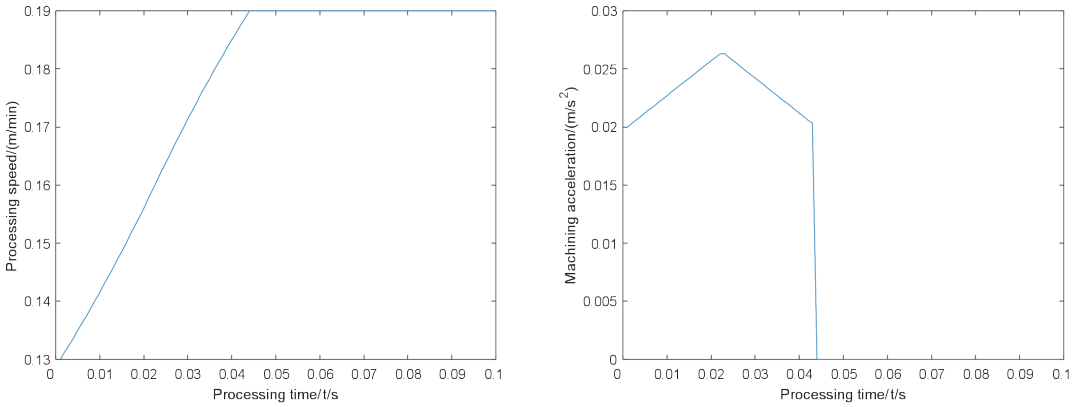

(a) (b)

Fig. 12. (Color online) Local machining speed and acceleration curves of AB segment: (a) curve of machining speed versus machining time in AB section and (b) curve of machining acceleration versus machining time in AB section.

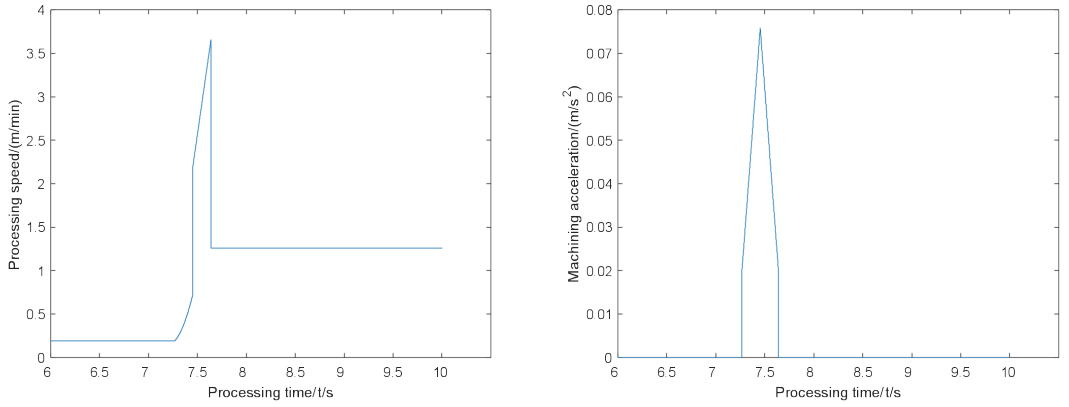

(a) (b)

Fig. 13. (Color online) Local machining speed and acceleration curves of BC segment: (a) curve of machining speed vs. machining time in BC section and (b) curve of machining acceleration vs. machining time in BC section.

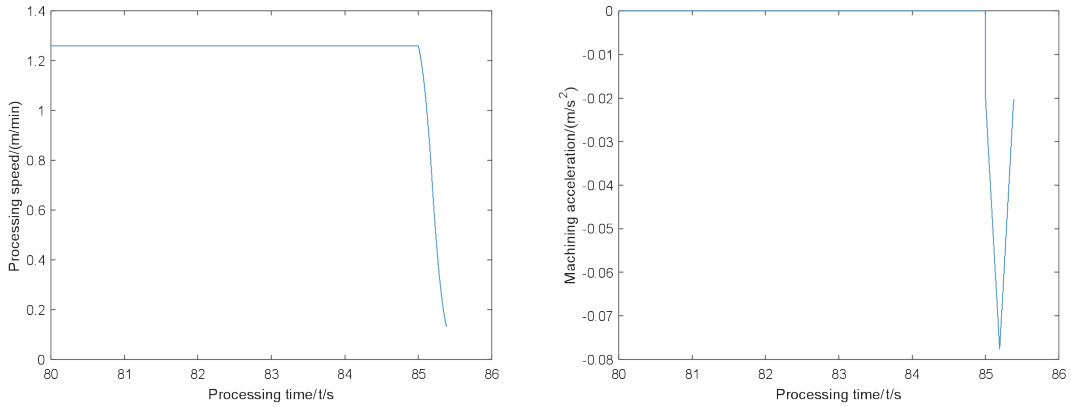

(a) (b)

Fig. 14. (Color online) Processing speed and acceleration curves of JK segment: (a) curve of machining speed versus machining time in JK section and (b) curve of machining acceleration versus machining time in JK section.

6. Discussion

The multisensor fusion S-curve acceleration and deceleration control model proposed in this study performs better than the traditional circular arc transition algorithm in terms of trajectory connection smoothness and processing time optimization. However, its curvature adaptability in complex surface machining still needs to be improved. The current model assumes that sensor data is real-time and noise-free, but in actual machining, sensor delays may lead to a lag in speed adjustment. In the future, the Kalman filter algorithm can be introduced to optimize the accuracy of data fusion. In addition, there is still room for optimizing the machining error of the circular arc transition algorithm in small-radius curve segments. The effect of tool wear on the trajectory can be predicted by combining deep learning. This model has significant application value in the machining of high-precision components of green converter stations (such as silicon steel sheets of converter transformer cores) and can be extended to the field of new energy equipment manufacturing. The follow-up research will focus on the multi-axis linkage machining scenario to further verify the effectiveness of the model in 3D complex trajectories.

7. Conclusions

In this paper, an arc transfer algorithm was proposed, through which the maximum transfer speed allowed under the condition of satisfying the machining error can be obtained, which can make the tool move in the direction before the moving speed drops to zero, that is, before reaching the inflection point.

Acknowledgments

This work was supported by the Digital Operation (Personalization) Construction Project of China Southern Power Grid Co., Ltd. under Grant no. 011000HK23110002.

References

1 D. F. Zhou and Q. Guan: Chem. Autom. Instrum. **45** (2018) 1. https://doi.org/10.3969/j.issn.1000-3932.2018.10.014 (in Chinese).
2 Y. K. Li and Y. M. Lv: Comb. Mach. Tools Autom. Mach. Technol. **1** (2017) 16. https:/doi.org/10.13462/j.cnki.mmtamt.2017.01.005 (in Chinese).
3 X. C. Shu, X. L. Huang, and R. H. Zhu: J. Jining Univ. **39** (2018) 4. https://doi.org/10.3969/j.issn.1004-1877.2018.05.002 (in Chinese).
4 G. B. Xu and D. Y. Yu: Control Eng. China (2017) 2053. https://doi.org/10.14107/j.cnki.kzgc.160316 (in Chinese).
5 H. H. Pan, Z. Q. Yang, L. Chen, H. T. Dong, H. Q. Tan, and W. Zhong: Mech. Sci. Technol. Aerosp. Eng. (2015) 1024. http://dx.doi.org/10.13433/j.cnki.1003-8728.2015.0710
6 J. X. Xiao, H. Zhang, B. G. Li, and G. L. Li: Comput. Integr. Manuf. Syst. (2019) 2248. http://dx.doi.org/10.13196/j.cims.2019.09.012 (in Chinese).
7 T. C. Lu and S. L. Chen: Int. J. Adv. Manuf. Technol. (2016) 219. https://doi.org/10.1007/s00170-016-8464-0
8 T. Wang, L. Chen, and Z. W. Guo: Comput. Integr. Manuf. Syst. (2019) 2648. https://doi.org/10.13196/j.cims.2019.10.023
9 M. Barton, M. Bizzarri, M. Rist, F. Sliusarenko, and O. Pottmann: ACM Trans. Graph **40** (2021) 1. https://doi.org/10.1145/3450626.3459837
10 H. H. Pan, Z. Q. Yang, and L. Chen: J. Mech. Eng. (2015) 151. https://doi.org/10.3901/JME.2015.05.151 (in Chinese).
11 J. Zhang, L. Q. Zhang, and K. Zhang: Chin. J. Mech. Eng. (2015) 2089. https://www.cmemo.org.cn/EN/Y2015/V26/I15/2089
12 X. Du, J. Huang, and L. Zhu: Procedia CIRP **56** (2016) 344. https://doi.org/10.1016/j.procir.2016.10.037
13 F. M. Lin and X. H. Ma: J. Syst. Sci. Math. Sci. **38** (2018) 1213. https://doi.org/10.12341/jssms13468
14 J. X. Xiao, H. Zhang, and B. G. Li: Comput. Integr. Manuf. Syst. **25** (2019) 2248. https://doi.org/10.13196/j.cims.2019.09.012 (in Chinese).

About the Authors

Li Yang graduated from Harbin University of Technology in 2015. He currently works for the Ultra High Voltage Transmission Company Dali Bureau, China Southern Power Grid Co., Ltd. He is mainly engaged in the operation and management of high-voltage DC transmission automation technology. (1053125623@qq.com)

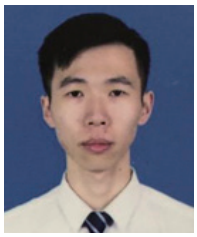

Zhou Guoen graduated from Guangdong University of Technology in 2020 and is currently employed at the Ultra High Voltage Transmission Company Dali Bureau, China Southern Power Grid Co., Ltd. He is mainly engaged in the operation and maintenance of high-voltage direct current transmission automation technology. (zhouguoen@im.ehv.csg)

Xue Jiaqi graduated with a bachelor's degree from Kunming University of Science and Technology in 2017. He is currently working in the Dali Bureau of China Southern Power Grid Ultra-High Voltage Transmission Company. He is mainly engaged in high-voltage DC transmission automation operation, maintenance, and management. (1146675042@qq.com)

Yang Junwei graduated from Guizhou Normal University in 2008 and is currently working for Longshine Technology Group Co., Ltd. He is mainly engaged in metered electricity consumption, load management and demand response, energy big data center, and vehicle-pile-grid cluster interaction. (yangjunwei@longshine.com; 357936645@qq.com)

Wang Wenting graduated from the Civil Aviation and Aviation College of Kunming University of Science and Technology. She is currently an intern at Longshine Technology Group Co., Ltd. (2100265702@qq.com)

Nie Tianyu is now studying in the Faculty of Information Engineering and Automation, Kunming University of Science and Technology. He is currently an intern at Longshine Technology Group Co., Ltd. (909778395@qq.com)